

A NOTE ON THE FINITE DEFORMATIONS OF A THICK ELASTIC SHELL OF REVOLUTION

J.T. ODEN, J.E. KEY,

*Division of Graduate Programs and Research,
The University of Alabama in Huntsville, Huntsville, Alabama, U.S.A.*

ABSTRACT

Finite deformations of a relatively thick highly elastic incompressible isotropic spherical shell subjected to external pressure are studied using the finite element method in conjunction with the method of incremental loading. Numerical results are presented and discussed.

1. INTRODUCTION

The theory of thin elastic shells emerged from the writings of Kirchhoff and Love in the nineteenth and early twentieth centuries and has reached a high degree of development in modern times. Much of the literature in recent years has dealt with various difficulties encountered when one or more of the classical Kirchhoff-Love hypotheses has been removed. For example, there has been considerable interest in the influence of transverse and extensional strains on the stresses and displacements of thin shells, the effects of transverse shear in thick shells wherein the Kirchhoff hypothesis is not strictly valid, and in the important problems of finite rotations, stability, and post buckling behavior. Until recently, each of these problems were attacked using a separate and often independent approximate shell theory because the use of a completely general theory is typically regarded as beyond the scope of contemporary methods of mathematical analysis. Indeed, insofar as the authors are aware, no solutions, either exact or approximate, exist for the problem of finite deformations (including finite strains and rotations) of thick or thin shells of revolution. Consequently, no data is available to assess the validity of the approximate theories mentioned previously, especially when all of the special effects are included simultaneously.

As a preliminary step toward resolving this problem, this paper is devoted to the approximate analysis of symmetric, arbitrarily large deformations of a thick, highly elastic shell-of-revolution. A thick spherical cap is analyzed using the finite-element method as an elastic body of revolution. The thickness is modelled using layers of triangular elements, and no restrictions are placed on the magnitudes of the strains, the degree of transverse extensional strain, the degree of extensional strain, the magnitude or variation of transverse shear strains, the use of conservative loads, or the magnitude of rotations. A representative example is presented and numerical solutions are analyzed. The limitations of various conventional assumptions in shell theory are made clear in this analysis.

2. FINITE ELEMENT MODEL OF SHELL OF REVOLUTION

We consider an incompressible isotropic hyperelastic body of revolution subjected to finite axisymmetric deformations about its axis of symmetry, x^3 . In convected cylindrical coordinates, the components of the second Piola-Kirchhoff stress tensor σ^{ij} are

$$\begin{aligned} \sigma^{\alpha\beta} &= 2 \frac{\partial W}{\partial I_1} \delta^{\alpha\beta} + 2 \frac{\partial W}{\partial I_2} [\delta^{\alpha\beta} (1 + \lambda^2) + 2 \epsilon^{\alpha\lambda} \epsilon^{\beta\mu} \gamma_{\lambda\mu}] + 2h\lambda^2 (\delta^{\alpha\beta} + 2 \epsilon^{\alpha\lambda} \epsilon^{\beta\mu} \gamma_{\lambda\mu}) \\ \sigma^{33} &= 0 \quad , \quad \sigma^{33} = \frac{1}{r^2} [2 \frac{\partial W}{\partial I_1} + 4(1 + \gamma_\alpha^\alpha) \frac{\partial W}{\partial I_2} + 2h\varphi] \end{aligned} \quad (1)$$

Here $\alpha, \beta, \lambda, \mu = 1, 2$, W is the strain energy per unit undeformed volume, I_1 and I_2 are the principal invariants of Green's deformation tensor, λ is the circumferential extension ratio, $\epsilon^{\alpha\lambda}$ is the two-dimensional permutation symbol, $\gamma_{\lambda\mu}$ are the components of the Green-Saint Venant strain tensor, h is the hydrostatic pressure, r is the radial coordinate, and φ is a scalar dependent on the strains. If u_1 and u_2 denote the radial and axial components of displacement, we find that

$$\begin{aligned} 2\gamma_{\alpha\beta} &= u_{\alpha,\beta} + u_{\beta,\alpha} + u_{\lambda,\beta} u_{\alpha,\lambda} \\ \gamma_{33} &= 0 \\ \gamma_{33} &= \frac{r^2}{2} (\lambda^2 - 1) \quad \lambda = 1 + \frac{u_1}{r} \end{aligned} \quad (2)$$

and

$$\begin{aligned} I_1 &= 2(1 + \gamma_\alpha^\alpha) + \lambda^2 \quad I_2 = 2\lambda^2(1 + \gamma_\alpha^\alpha) + \varphi \\ I_3 &= \lambda^2\varphi = 1 \end{aligned} \quad (3)$$

where

$$\varphi = 1 + 2\gamma_\alpha^\alpha + 2\epsilon^{\alpha\beta} \epsilon^{\lambda\mu} \gamma_{\alpha\lambda} \gamma_{\beta\mu} \quad (4)$$

To obtain a finite element model of the body, we divide it into a collection of triangular elements, as shown by Oden and Key [1], and approximate the displacement fields locally over each element e by functions of the form

$$u_\alpha = \psi_N(\underline{x}) u_\alpha^N \quad (5)$$

where N is summed from 1 to 3, u_α^N are the values of u at node N of the element, and

$$\begin{aligned} \psi_N(\underline{x}) &= a_N + b_{N\alpha} x^\alpha \\ a_N &= \frac{1}{4A_0} \epsilon_{NMK} \epsilon_{\lambda\mu} x_N^\lambda x_K^\mu \\ b_{N\alpha} &= \frac{1}{2A_0} \begin{bmatrix} x_2^2 - x_3^2 & x_3^1 - x_2^1 \\ x_3^2 - x_1^2 & x_1^1 - x_3^1 \\ x_1^2 - x_2^2 & x_2^1 - x_1^1 \end{bmatrix} \end{aligned} \quad (6)$$

Here A_0 is the area of the element and x_M^α are the local coordinates of node M. Denoting by $p_{N\alpha}$ the components of generalized force at node N due to body forces F_α and surface tractions S_α , i.e.

$$p_{N\alpha} = \int_{V_0} \psi_N F_\alpha dV_0 + \int_{S_0} S_\alpha \psi_N dS \quad (7)$$

and following the usual procedure of minimizing the potential energy locally over the element, we obtain for the governing equations

$$p_{N\alpha} = 2v_0 \left(\frac{\partial W}{\partial I_1} + \lambda^a \frac{\partial W}{\partial I_2} \right) \frac{\partial \gamma_\beta^\beta}{\partial u_N^\alpha} + v_0 \left[\frac{\partial W}{\partial I_1} + 2(1 + \gamma_\beta^\beta) \frac{\partial W}{\partial I_2} + h\varphi \right] \frac{\partial \lambda^a}{\partial u_N^\alpha} + v_0 \left(\frac{\partial W}{\partial I_1} + \lambda^a h \right) \frac{\partial \varphi}{\partial u_N^\alpha} \quad (8)$$

where, approximately,

$$\begin{aligned} \frac{\partial \gamma_\beta^\beta}{\partial u_N^\alpha} &= b_{N\beta} (\delta_\alpha^\beta + b_{M\beta} u_M^\alpha) \\ \frac{\partial \lambda^a}{\partial u_N^\alpha} &= 2 \frac{\lambda}{\bar{r}} (\delta^{N1} + \delta^{N2} + \delta^{N3}) \delta^{\alpha 1} \\ \frac{\partial \varphi}{\partial u_N^\alpha} &= 2b_{N\lambda} (\delta_\alpha^\beta + b_{M\beta} u_M^\alpha) [\delta_{\beta\lambda} + \gamma_{\rho\mu} (\epsilon^{\beta\rho} \epsilon^{\lambda\mu} + \epsilon^{\rho\lambda} \epsilon^{\mu\beta})] \end{aligned} \quad (9)$$

Here \bar{r} is the mean nodal radius, $(r_1 + r_2 + r_3)/3$. Assuming that the hydrostatic pressure is uniform over the element, we also establish the discrete incompressibility condition,

$$\pi(\bar{r} + \bar{u}_1) \left| \sum_{p=1}^3 \epsilon^{MNP} \epsilon_{\alpha\beta\gamma} (x_M^\alpha + u_M^\alpha) (x_N^\beta + u_N^\beta) \right| = v_0 \quad (10)$$

where $\bar{u}_1 = (u_1^1 + u_1^2 + u_1^3)/3$ and v_0 is the initial volume of the element.

The remainder of the formulation is essentially the same as that discussed by Oden and Key [1],[2] and Oden [3]. Elements are connected together to form the discrete model of the body, and we obtain systems of nonlinear equations of equilibrium and incompressibility in the nodal displacements and element hydrostatic pressures. These are solved using the incremental loading technique described by Oden [3]. Also, account is made of the fact that the generalized forces $p_{N\alpha}$ depend, in general, on the deformation and orientation of the element. The procedure described in [4] is used to depict such loads.

3. NUMERICAL ANALYSIS AND RESULTS

Spherical Shell. We now apply the finite-element model developed in the previous section to the analysis of a spherical shell composed of an isotropic incompressible material of the Mooney type;

$$W = C_1 (I_1 - 3) + C_2 (I_2 - 3) \quad (7)$$

In the present example, we take $C_1 = 80 \text{ lbs./in.}^2$ and $C_2 = 20 \text{ lbs./in.}^2$. The material is thus assumed to be capable of sustaining very large strains and still behaving elastically.

The undeformed geometry of the shell under investigation is shown in Fig. 1a. The shell represents a shallow spherical cap with an internal radius of 15.0 in.; the shell rises 2.0 in. in a span of 15.0 in. and the thickness-radius ratio, t/R , is 0.053. We apply a uniform pressure p over the exterior surface of the shell, and we confine our attention to deformations symmetric with respect to the axis of revolution of the spherical segment. A finite-element model of the shell obtained using triangular elements-of-revolution is shown in Fig. 1b. The thickness is modeled using 8 triangles, which should be very adequate to depict transverse shear and bending deformations.

Incremental Loading. The finite-element analysis of the shell problem described above involves the solution of 183 simultaneous nonlinear equilibrium equations in 103 unknown nodal displacements and 80 hydrostatic pressures. They were solved using the method of incremental loading. Complete details of this method are given by Oden and Key [2] and Oden [3]; however, for the sake of completeness, we outline briefly the essential features here.

Consider the system of nonlinear equations

$$\underline{f}(\underline{X}, p) = \underline{0} \quad (8)$$

where \underline{f} is an n -vector of nonlinear equations in \underline{X} , \underline{X} being an n -vector of unknown generalized displacements and hydrostatic pressures, and p is a parameter corresponding to the load. Assuming, for the moment, that \underline{X} and p are functions of some dummy parameter t , we compute

$$\dot{\underline{f}} = \underline{0} = \underline{J}(\underline{X}, p)\dot{\underline{X}} + \underline{g}(\underline{X}, p)\dot{p} \quad (9)$$

where

$$J_{ij} = \partial f_i / \partial X_j, \quad g_i = \partial f_i / \partial p \quad (10)$$

We then proceed to integrate the system of differential equations (9).

The numerical results described below were obtained using a corrector-predictor scheme based on Euler's method and the Newton-Raphson method. That is, the $r + 1$ st iterate is given by

$$\underline{X}^{r+1} = \underline{X}^r - \underline{J}(\underline{X}^r, p^r)^{-1} \underline{g}(\underline{X}^r, p^r) \delta p \quad (11)$$

where δp is the prescribed load increment and p^r is the load level after r increments are applied. For each r , a sequence of Newton-Raphson iterations are then performed until the equilibrium equations are satisfied for a given p^r within an error limit of $\max_i |\Delta X_i| \leq 0.1$. Singularities in the jacobian $\underline{J}(\underline{X}, p)$ were determined approximately by testing the number m of N.R. iterations required to reduce the error within the prescribed limit. Near singularities, increments $\Delta \underline{X}$ were held fixed and N.R. iterations were performed until a load was reached that satisfied the equilibrium equations. In such cases, tests were run to determine the appropriate sign of δp for subsequent load increments. This process enables

one to compute the entire quasi-static history of the response due to a sequence of increments of loading and to generate multivalued solutions, bifurcations, etc.

Numerical Results. Figures 2-9 contain samples of the numerical results obtained in this investigation. In Fig. 2 is seen the computed deflected profile of the shell for various values of external pressure. For the particular geometry and material properties considered, the shell response was essentially linear (e.g., small displacements, infinitesimal strains) for pressures from 0 to approximately 0.1 psi. With increases in pressure beyond 0.1 psi, large displacements and rotations were introduced. The vertical displacement of the crown reached 1.10 in. (slightly greater than the shell's undeformed thickness) at $p = 2.5$ psi. While displacements are "large" in the usual sense at this level of pressure, transverse shearing strains, transverse extensional strains, and extensional strains of the middle surface are still very small. At a pressure of around 2.52 psi, the shell equilibrium became unstable and the initiation of the "snap-through" phenomenon is observed. The external pressure required to maintain equilibrium decreased markedly with an increase in the center displacement beyond this point: when the crown displacement w reached 4.0 in., the pressure was reduced to zero and a negative pressure was computed for $4.0 \leq w \leq 4.7$ in. At this level of pressure, very large rotations are experienced, the rotation at the support being around 44° . Transverse extensional strains at the crown reach 10 percent at this point. At $w > 5.0$ in., the curvature of the shell has completely changed from concave to convex and stresses in the top fibers change from compression to tension. Beyond $w = 4.0$ in., extensional strains of the middle surface become quite pronounced, and at $w = 5.0$ in., the maximum extensional strain of the middle surface is 16 percent. We observe that at $p = 2.0$ psi ($w = 5.6$ in.) the bending strains have essentially disappeared and the shell behaves as a membrane. Further increases in pressure cause inflation of the membrane and, at $p = 20.0$ psi, the membrane assumes the balloon-like shape indicated in the figure.

An interesting feature of the response is that multiple solutions are obtained for a single pressure. This is illustrated in Fig. 3 wherein three distinct deformed configurations are shown for a pressure of 2.0 psi.

Figures 4, 5, and 6 show the pressure variation versus the displacements of representative nodal points. Figure 4 contains the variation of the vertical displacement of the outer nodal point at the crown while Figs. 5 and 6 contain the variation of the horizontal displacements of points located at the top and at the bottom, respectively, of a cross-section 15° from the support.

The computed variation of element hydrostatic pressures with external pressure is illustrated in Figs. 7, 8, and 9 for the three elements labeled A, B, and C respectively. It was observed that the rate of convergence for displacement unknowns was approximately 10 times faster than that of the hydrostatic pressures. In future work, scaling of the unknowns may prove to be rewarding in saving computer time.

The problem discussed here required approximately 10 hours of computing time on the UNIVAC 1108 digital computer.

Acknowledgement. Support of the work reported in this paper by the U. S. Air Force Office of Scientific Research under Contract F44620-69-C-0124 is gratefully acknowledged.

REFERENCES

- [1] ODEN, J. T. and KEY, J. E., "Numerical Analysis of Finite Axisymmetric Deformations of Incompressible Elastic Solids of Revolution", International Journal of Solids and Structures 6, 497-418 (1970).
- [2] ODEN, J. T. and KEY, J. E., "Analysis of Finite Deformations of Elastic Solids by the Finite Element Method", Proceedings, IUTAM Symposium on High-Speed Computing of Elastic Structures, Liege, 1970.
- [3] ODEN, J. T., Finite Elements of Nonlinear Continua, McGraw-Hill Book Co. (1971).
- [4] ODEN, J. T., "On an Approximate Method for Computing Nonconservative Generalized Forces on Finitely Deformed Finite Elements", AIAA Journal 8, 2088-2090 (1970).

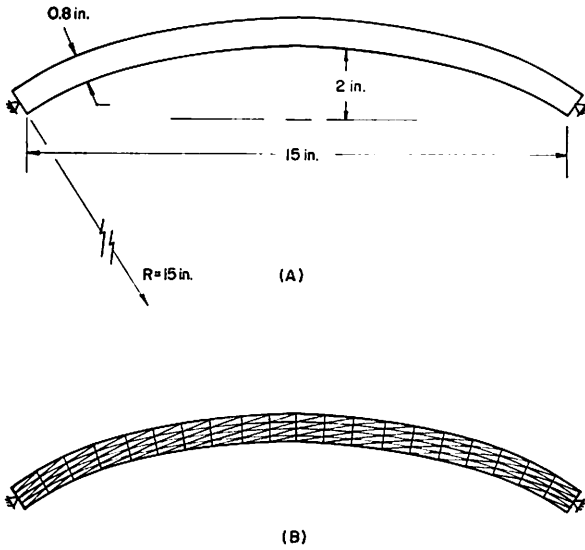


Figure 1. Spherical shell and a finite element model of the shell.

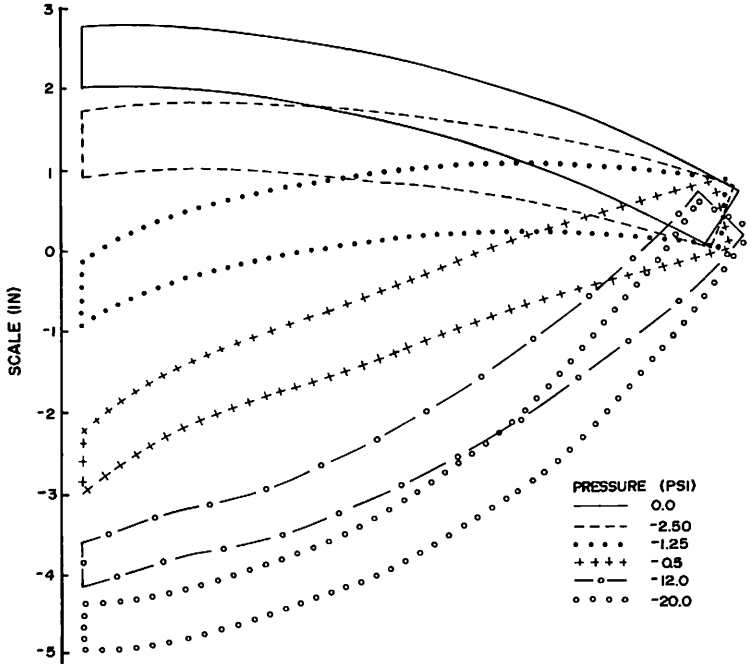


Figure 2. Computed deformed profiles of the shell for various values of external pressure.

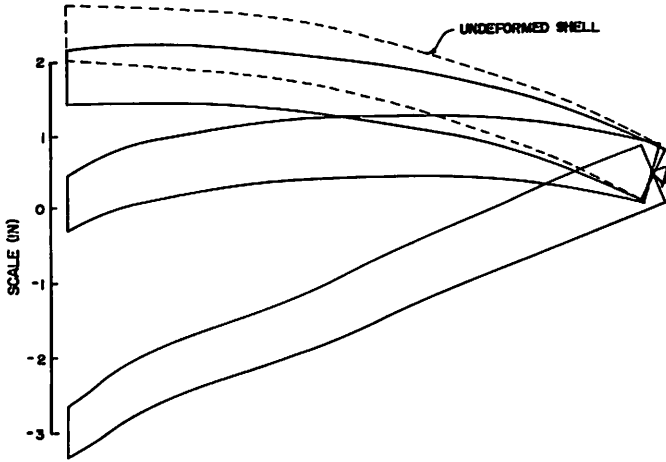


Figure 3. Three deflected profiles at a pressure of 2 psi.

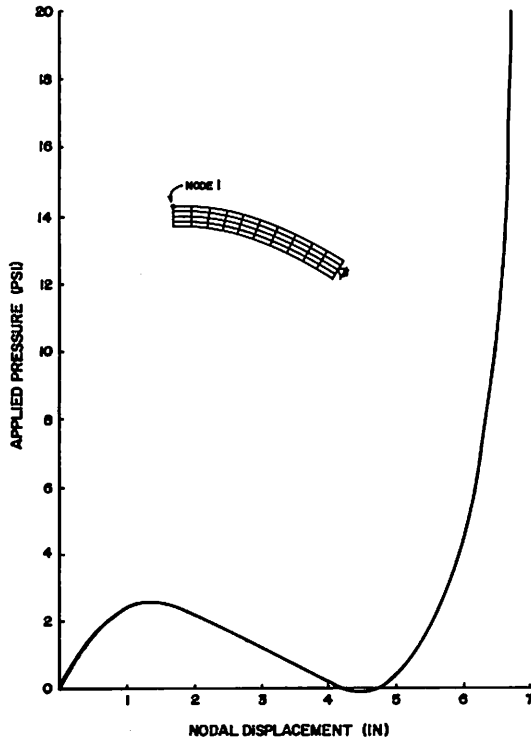


Figure 4. Computed variation of vertical displacement of node 1 with applied pressure.

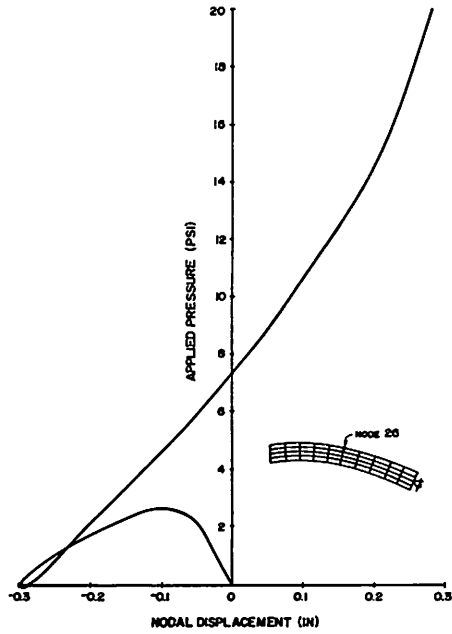


Figure 5. Computed variation in horizontal displacement of node 26 with applied pressure.

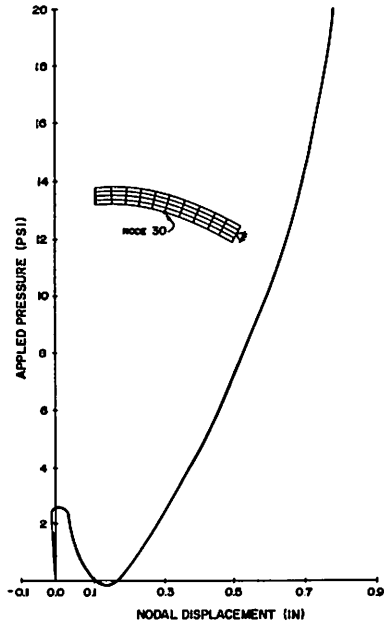


Figure 6. Computed variation in horizontal displacement of node 30 with applied pressure.

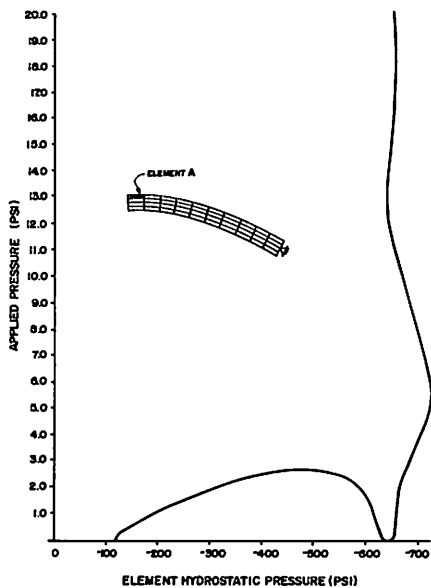


Figure 7. Computed variation in element hydrostatic pressure with applied pressure, element A.

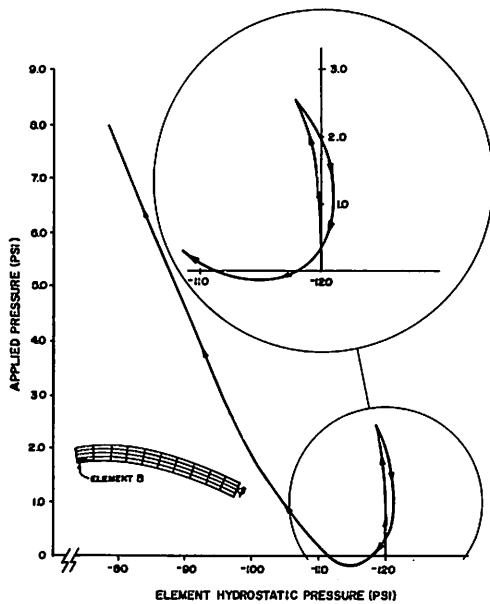


Figure 8. Computed variation of element hydrostatic pressure with applied pressure, element B.

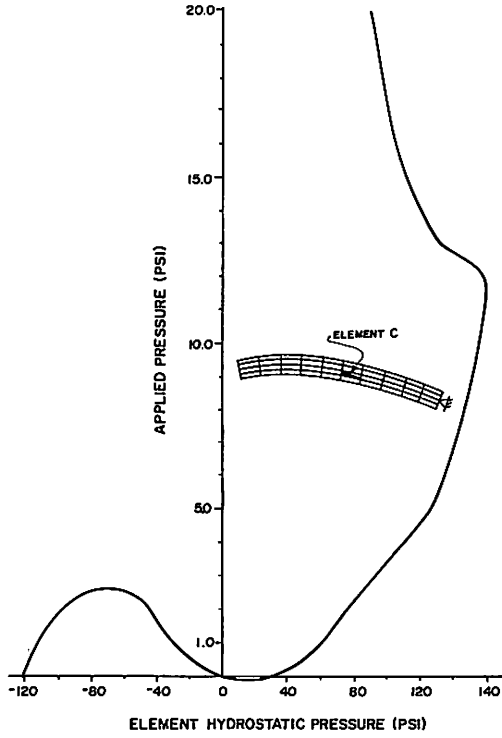


Figure 9. Computed variation in element hydrostatic pressure with applied pressure, element C.

DISCUSSION

Q K. WILLAM, Germany

1. The importance of rigid body modes + constant strain states can be considerable (see Cantin, AIAA 1969).
2. Are more sophisticated tests for non-conservative loadings available ?
3. How does your incremental formulation account for non-conservative loads ?

A J. T. ODEN, U. S. A.

1. Concerning the first comment, I am well aware of the Cantin-Clough paper. One can always produce geometries and loadings wherein the inclusion of rigid motions considerably improves the results. However, for completeness and convergence, they are definitely not needed. This can be shown rigorously (see my forthcoming book, McGraw-Hill, 1971).
2. As for more sophisticated tests for non-conservative loads, I dealt with several of these in a recent AIAA technical note.
3. Finally, concerning the incremental load calculation of non-conservative forces, these are computed consistently from the actual loading state on deformed material surface areas. These are known in terms of the nodal displacements on the surface. I discuss this calculation in some detail in the references listed at the end of the paper.

Q G. S. DHATT, Canada

Rigid body motions and constant strain requirements are generally important to include for curved element in order to have better convergence. How far are these requirements influential in non-linear formulations for better convergence ?

A J. T. ODEN, U. S. A.

My response to this question can be divided into two parts: First, rigid body motions and constant strains are reducible in the elements used in my analysis. I see no problems concerning the inclusion of rigid motion in an element that is not essentially present, in a perhaps simpler form, in linear analysis. Secondly, I should say that such rigid modes and constant strains are actually not needed for acceptable elements. Indeed, the overriding criterion for conforming elements is completeness which need not be equivalent to the requirements of rigid motion and constant strains.

Q M. J. MIKKOLA, Finland

Have you noticed differences in convergence rate between elements including rigid-body motion and constant strain and elements including complete set of functions, in particular in curved shell elements ?

J. T. ODEN, U. S. A.

A No, I have not. But I can refer you to several papers in which it is stressed that the inclusion of rigid motion does indeed increase the rate of convergence. This makes sense intuitively, since an acceptable element without rigid motion might lead to very large systems of equations before desired results are produced - in other words, in deformations involving appreciable rigid motion, elements containing rigid motions would obviously start closer to the solution than those which did not. Rates of convergence, in the usual sense of the term "rate", might not be influenced at all.